Eur. Phys. J. B **14**, 617–625 (2000)

THE EUROPEAN PHYSICAL JOURNAL B

EDP Sciences
© Società Italiana di Fisica
Springer-Verlag 2000

Temperature dependence of infrared conductivity of manganites $Pr_{0.7}Ca_{0.3-x}Sr_xMnO_3$ (x = 0, 0.05 and 0.2)

N. Petit[1,a], C. Daulan[1], J.-C. Soret[1], A. Maignan[2], and F. Gervais[1]

[1] Laboratoire d'Électrodynamique des Matériaux Avancés[b], Faculté des Sciences & Techniques, Université François Rabelais, 37200 Tours, France
[2] CRISMAT[c], ISMRA, boulevard Maréchal Juin, 14050 Caen, France

Received 20 July 1999 and Received in final form 15 October 1999

Abstract. The temperature dependence of the reflectivity spectra of three manganites ceramics with compositions $Pr_{0.7}Ca_{0.3}MnO_3$, $Pr_{0.7}Ca_{0.25}Sr_{0.05}MnO_3$ and $Pr_{0.7}Ca_{0.1}Sr_{0.2}MnO_3$ has been investigated by infrared reflectivity spectroscopy in the wave number range 0.005–1.1 eV. The compound $Pr_{0.7}Ca_{0.25}Sr_{0.05}MnO_3$ which shows the largest conductivity jump at the ferromagnetic-paramagnetic phase transition has been studied in details. The optical conductivity of this compound is deduced from the best fit to reflectivity spectra of a "double-damping Drude" model, itself derived from the factorized form of the dielectric function. Excellent agreement with Kramers-Kronig transformation is reported. The model allows in particular to discriminate the contributions to the optical conductivity of trapped charges (polarons) and mobile charge carriers.

PACS. 71.30.+h Metal-insulator transitions and other electronic transitions – 75.70.Pa Giant magnetoresistance – 78.30.-j Infrared and Raman spectra

1 Introduction

Manganese oxides of composition $Ln_{1-x}A_xMnO_3$ (where Ln and A are rare-earth and alkaline-earth elements, respectively) are the object of considerable interest because of their fascinating electronic and magnetic properties [1,2]. In particular, for compositions corresponding to $x = 0.3$, colossal magneto-resistance (CMR) is observed near the Curie temperature T_C [3–5]. The properties of these compounds [6] can be monitored *via* at least three factors which may interact:

- the external cation size (the "A-type" cation of the general formula of oxidic perovskite ABO_3) and possible cation mismatches, which, among other effects, control the internal chemical pressure and shifts the electronic band structure;
- the external cation average valence which controls the Mn^{3+}/Mn^{4+} ratio and, therefore, the magnetic structure;
- the number of charge carriers which plays a major role in the conductivity, and which depends on the average valences at both cationic sites, and also on the oxygen stoichiometry.

Considering the role of the first factor upon CMR phenomena for example, by decreasing the size of the average A site on varying x from 0.2 to 0.05 in the series $Pr_{0.7}Ca_{0.3-x}Sr_xMnO_3$, the resistance ratio defined as $R(H = 0)/R(H = 7\ \mathrm{T})$ is increased, by as much as four magnitude orders whereas T_C decreases from 200 K to 85 K [3–6]. In the manganites, a dynamic Jahn-Teller effect of the manganese ion is suspected to play a role in their unusual properties. The Jahn-Teller effect implies a strong electron-phonon interaction so that polarons may be involved as suggested in several papers [7–11]. As far as oxides of transition metal elements are concerned, polarons have already been identified in the mid-infrared region of the spectral conductivity of Pr_2NiO_4 [12,13] and are suspected in cuprates too [14,15]. Similar to cuprates and nickelates, it is tempting to investigate the infrared conductivity of manganites and check whether or not the spectral conductivity would display species interpretable in terms of polarons, as suggested in previous papers [16–23]. The magneto-transport properties of the compounds of the series $Pr_{0.7}Ca_{0.3-x}Sr_xMnO_3$ have already been widely studied with conventional techniques [3–5], but not by optical conductivity for $0 \leq x \leq 0.20$ to the best of our knowledge. The compounds $x = 0$, 0.05 and 0.2 are studied here under sintered ceramics form. The compounds $x = 0.2$ and $x = 0.05$ show a transition from a low-temperature ferromagnetic (FM) metal-like phase to a high temperature paramagnetic semi-conductor

[a] e-mail: petit@delphi.phy.univ-tours.fr
[b] LRC M01 associated to Commissariat à l'Énergie Atomique, FRE 2077 associated to CNRS
[c] UMR 6508

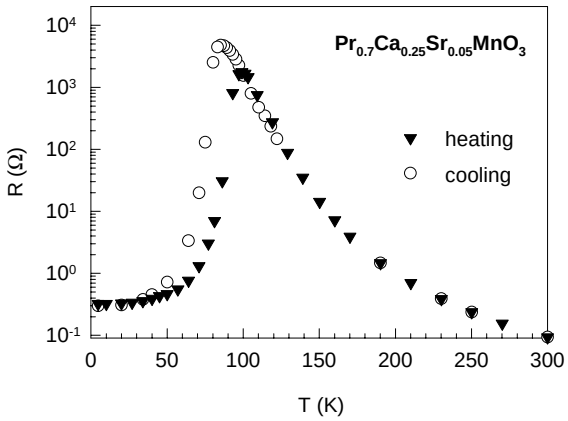

Fig. 1. Temperature dependence of resistance measured upon cooling (open circles) and heating (filled triangles) for the compound $Pr_{0.7}Ca_{0.25}Sr_{0.05}MnO_3$. Note hysteresis.

like one. The onset of the phase transition temperature are observed at $\sim$ 200 K and $\sim$ 100 K for $x = 0.2$ and $x = 0.05$, respectively. The paper focuses upon the sample $x = 0.05$ for which the onset of the transition temperature is here obtained upon heating. The hysteresis shifts the onset temperature down to 86 K upon cooling (Fig. 1). Conversely, the compound with $x = 0$ exhibits a semi-conducting behavior in the whole studied temperature range as shown by resistivity curve [6]. Optical conductivity spectroscopy is most useful for the investigation of the electronic structures of the compounds with electron correlations, and the exploration of the electronic charge dynamics. Inspection of literature shows that all papers in this field perform a Kramers-Kronig transformation of reflectivity data [16–26]. This method assumes the knowledge of the reflectivity from zero to infinite frequency, what is obviously not feasible. In insulating media, the knowledge of spectral data in the energy range of non-zero dispersion is sufficient. In conducting media, however, there is remaining dispersion down to zero frequency. We will confirm that such materials do not behave like normal metals. An extrapolation of spectral data down to zero with a model inherited from normal metals, such as Drude or Hagen-Rubens, prior Kramers-Kronig transformation is, therefore, somewhat hazardous. Conversely, it is surprising to see that very few authors [16,27] attempted to fit the reflectivity spectra as it is currently the case in literature for other classes of materials, presumably because current models hardly work. A parametrisation of the spectra allows easier comparison with other classes of non-metal conducting materials and, therefore, appears worth attempting. In the absence of satisfactory results upon applying a conventional Drude model for the charge carriers and usual phonon oscillator, we will apply the "double-damping-Drude model" already found to fit the spectra of other conducting oxides. This model will be shown to be able to parameterize both reflectivity and conductivity of the manganite sample with $x = 0.05$ *vs.* temperature, satisfactorily.

2 Infrared conductivity and double-damping Drude model

The temperature dependence of infrared reflectivity spectra of a number of conducting oxides was investigated in previous papers [28–30]. It was shown in most of them that the conventional Drude model

$$\tilde{\varepsilon}(\omega) = \varepsilon_\infty \left[1 - \frac{\Omega_\mathrm{p}^2}{\omega(\omega - \mathrm{i}\gamma)}\right] \tag{1}$$

is unable to fit the experimental reflectivity

$$R(\omega) = \left|\left(\sqrt{\tilde{\varepsilon}(\omega)} - 1\right) \Big/ \left(\sqrt{\tilde{\varepsilon}(\omega)} + 1\right)\right|^2 \tag{2}$$

of any conducting oxide, correctly. This non-Drude behavior is a first indication of the unconventional character of the spectral conductivity $\tilde{\sigma}(\omega)$ of oxides, itself related to the dielectric function $\tilde{\varepsilon}(\omega)$, *via*

$$\tilde{\varepsilon}(\omega) = 1 - \frac{\mathrm{i}\tilde{\sigma}(\omega)}{\varepsilon_\mathrm{v}\omega}\,. \tag{3}$$

One way to overcome the difficulty of very poor fit with the conventional Drude model, was the introduction [28–30] of a double-damping-Drude term in the form

$$\tilde{\varepsilon}(\omega) = \varepsilon_\infty \left[1 - \frac{\Omega_\mathrm{p}^2 + \mathrm{i}(\gamma_\mathrm{p} - \gamma_0)\omega}{\omega(\omega - \mathrm{i}\gamma_0)}\right] \tag{4}$$

(in the absence of phonons or other oscillators). The above formula reduces to the simple Drude expression (1) when $\gamma_\mathrm{p} = \gamma_0$. Here γ_p represents the linewidth of the plasma response centered at $\omega = \Omega_\mathrm{p}$. γ_0 is the linewidth of the Drude-like absorption peak centered at $\omega = 0$.

Using equations (3, 4), the double-damping-Drude conductivity is expressed as

$$\tilde{\sigma}(\omega) = \varepsilon_\mathrm{v}\varepsilon_\infty \frac{(\gamma_\mathrm{p} - \gamma_0)\omega - \mathrm{i}\Omega_\mathrm{p}^2}{\omega - \mathrm{i}\gamma_0} \tag{5}$$

and then the real part of the conductivity, $\sigma(\omega)$ can be written as

$$\sigma(\omega) = \varepsilon_\mathrm{v}\varepsilon_\infty \frac{\Omega_\mathrm{p}^2\gamma_0}{\omega^2 + \gamma_0^2} + \varepsilon_\mathrm{v}\varepsilon_\infty \frac{(\gamma_\mathrm{p} - \gamma_0)\omega^2}{\omega^2 + \gamma_0^2}\,. \tag{6}$$

The first term is the conventional Drude contribution with a Lorentzian profile while the second part represents an additional contribution that is assigned to incoherent scattering. Indeed, this term tends to zero when $\omega \to 0$, which means that it hardly contributes to the free carrier motion. Conversely, for an appropriate choice of parameters, this term reproduces a flat real conductivity as is observed experimentally in low-conductivity systems where incoherent scattering is suspected. In all these expressions, $\varepsilon_\infty = 1 + \chi_\mathrm{electronic}$ is the "high-frequency" dielectric constant from the viewpoint of the IR spectroscopist. Namely,

it takes into account the interband absorption, known to be located at higher energies (~ 1.5 eV and ~ 4.5 eV).

The model equation (4) was shown, for example, to be the only one to our knowledge, able to fit the reflectivity of $YBa_2Cu_3O_7$ in the infrared and visible range (nearly four orders of magnitude of energy) *with only 4 adjustable parameters* [31]. The model implicitly introduces a quadratic frequency dependence of a plasmon damping function [32]. This model is based upon the extension of the Lyddanne-Sachs-Teller relationship [33]

$$\tilde{\varepsilon}(\omega) = \varepsilon_\infty \prod_j \frac{\Omega_{j\mathrm{LO}}^2 - \omega^2 + \mathrm{i}\gamma_{j\mathrm{LO}}\omega}{\Omega_{j\mathrm{TO}}^2 - \omega^2 + \mathrm{i}\gamma_{j\mathrm{TO}}\omega}\,. \tag{7}$$

The model equation (7) was shown to be able to take into account all kinds of excitations, which are currently observed in conducting oxides (phonons, plasmon, polarons, superconducting condensate, relaxators, gaps, other mid-infrared bands.). It is a straightforward application of one of the Maxwell equation, which states that transverse optical (TO) modes are the complex poles of the dielectric function $\tilde{\varepsilon}(\omega)$, while longitudinal optical (LO) modes satisfy $\tilde{\varepsilon} = 0$, hence are the complex zeroes of $\tilde{\varepsilon}(\omega)$. Since there is no restoring force for the free electron motions, the TO frequency is set equal to zero, and equation (7) applied to the plasmon mode, reduces to equation (4). In the presence of phonons (or any other kind of oscillator) and plasmon in the same frequency range, the following expression has been shown to allow the separate determination of phonon and plasmon parameters [28–31].

$$\tilde{\varepsilon}(\omega) = \varepsilon_\infty \left[\prod_j \frac{\Omega_{j\mathrm{LO}}^2 - \omega^2 + \mathrm{i}\gamma_{j\mathrm{LO}}\omega}{\Omega_{j\mathrm{TO}}^2 - \omega^2 + \mathrm{i}\gamma_{j\mathrm{TO}}\omega} - \frac{\Omega_\mathrm{p}^2 + \mathrm{i}(\gamma_\mathrm{p} - \gamma_0)\omega}{\omega(\omega - \mathrm{i}\gamma_0)} \right]. \tag{8}$$

For weakly conducting samples, the major contributions to the dielectric response are polar phonons. But even for highly-conducting oxides, polar phonons are hardly screened by charge carriers. Normal metals show high reflectivity up to the cut-off plasma frequency that usually lies in the ultraviolet range. Conversely, in conducting oxides, the situation is entirely different with a plasma edge that hardly reaches the visible range and stays in the infrared. This is the reason of the black color of conducting oxides because visible light is absorbed by charge carriers but poorly reflected, and definitely not near 100% reflected like true metals. Another point that appears common to all conducting oxides is that the plasma response is highly damped, even overdamped in most cases. In addition to phonon and charge carrier response, each of the spectral response functions, reflectivity, dielectric function, optical conductivity, are sensitive to the motion (diffusive, relaxational, vibrational) of any charged particle (or atom). The model equation (8) is able to discriminate between motions with a restoring force like phonons or trapped polarons, and those without restoring forces like plasmon or mobile polarons.

3 Experiments

The infrared reflectivity spectra of the three samples studied were performed with an IFS 113 Bruker infrared Fourier-transform spectrometer. The $Pr_{0.7}Sr_{0.3-x}Ca_xMnO_3$ samples were sintered ceramics. They were prepared by thoroughly mixing Pr_6O_{11}, $SrCO_3$, CaO and MnO_2 in stoichiometric proportions. The mixtures were first heated at 950 °C, two times, with an intermediate grinding, to achieve decarbonatation. Powders were pressed in the form of pellets under 1 ton/cm^2 and sintered at 1500 °C for 12 h in air. The samples were then cooled at 5 °C/min down to 800 °C and, finally, quenched to room temperature. The density of the ceramics was found to be of about 80–85% of the theoretical value. In order to obtain bright smooth surfaces for the optical measurements the pellets have been polished by using successive abrasive disks of decreasing rugosity together with diamond pastes. To obtain a better polished surface than for the sample $Pr_{0.7}Ca_{0.1}Sr_{0.2}MnO_3$ (as discussed later on), the $Pr_{0.7}Ca_{0.3}MnO_3$ and $Pr_{0.7}Ca_{0.25}Sr_{0.05}MnO_3$ samples were polished with alumina paste of 2 μm-sized grains. Since these perovskites exhibit slightly distorted cubic structures, the infrared response is pseudo-isotropic, and the reflectivity of the ceramics is very similar to that of a single crystal. A recent study [25] performed with a single crystal of composition different from that investigated here has evidenced some difference between the polarisations parallel to the b and c axes, but only for the part of the spectra above 0.7 eV at 300 K and above 0.2 eV at 10 K. In particular, the anisotropy in the phonon region is so small that it is unobserved in reference [25]. At first, the infrared spectra of the $Pr_{0.7}Ca_{0.1}Sr_{0.2}MnO_3$ sample, shown in Figure 2a, were measured. Attempts to apply the simple phenomenological model presented in Section 2 to both reflectivity and conductivity *vs.* temperature were carried out [34]. But, by comparison with the spectra obtained later for $Pr_{0.7}Ca_{0.25}Sr_{0.05}MnO_3$ and $Pr_{0.7}Ca_{0.3}MnO_3$, it appears that the surface quality of the sample was not good enough to reflect light in proper specular conditions. Thus, the parameterization of these spectra was abandoned. Nevertheless it is worth considering the relative evolution of the reflectivity spectrum with temperature. As for the $Pr_{0.7}Ca_{0.25}Sr_{0.05}MnO_3$ sample (Fig. 2b), the reflectivity spectra exhibit a large dependence on temperature. Both compositions $x = 0.2$ and 0.05 show a similar behavior. At room temperature, the spectra are typical of semi-conductors with little-screened phonons. Globally, we discern three principal phonon peaks (or group of peaks) as expected for perovskite structure materials. By decreasing temperature, the reflectivity levels above the phonon region (> 0.1 eV) are lowered till T_C is reached (reflecting the lowering of the pseudo-Drude spectral weight) consistent with the semi-conducting behavior emphasized in the $R(T)$ curves for these compounds (Fig. 1 for $x = 0.05$). Below T_C, the spectra change continuously from a semi-conducting-like profile to a metallic-like one. The reflectivity spectra at various temperatures of the $Pr_{0.7}Ca_{0.3}MnO_3$ sample are

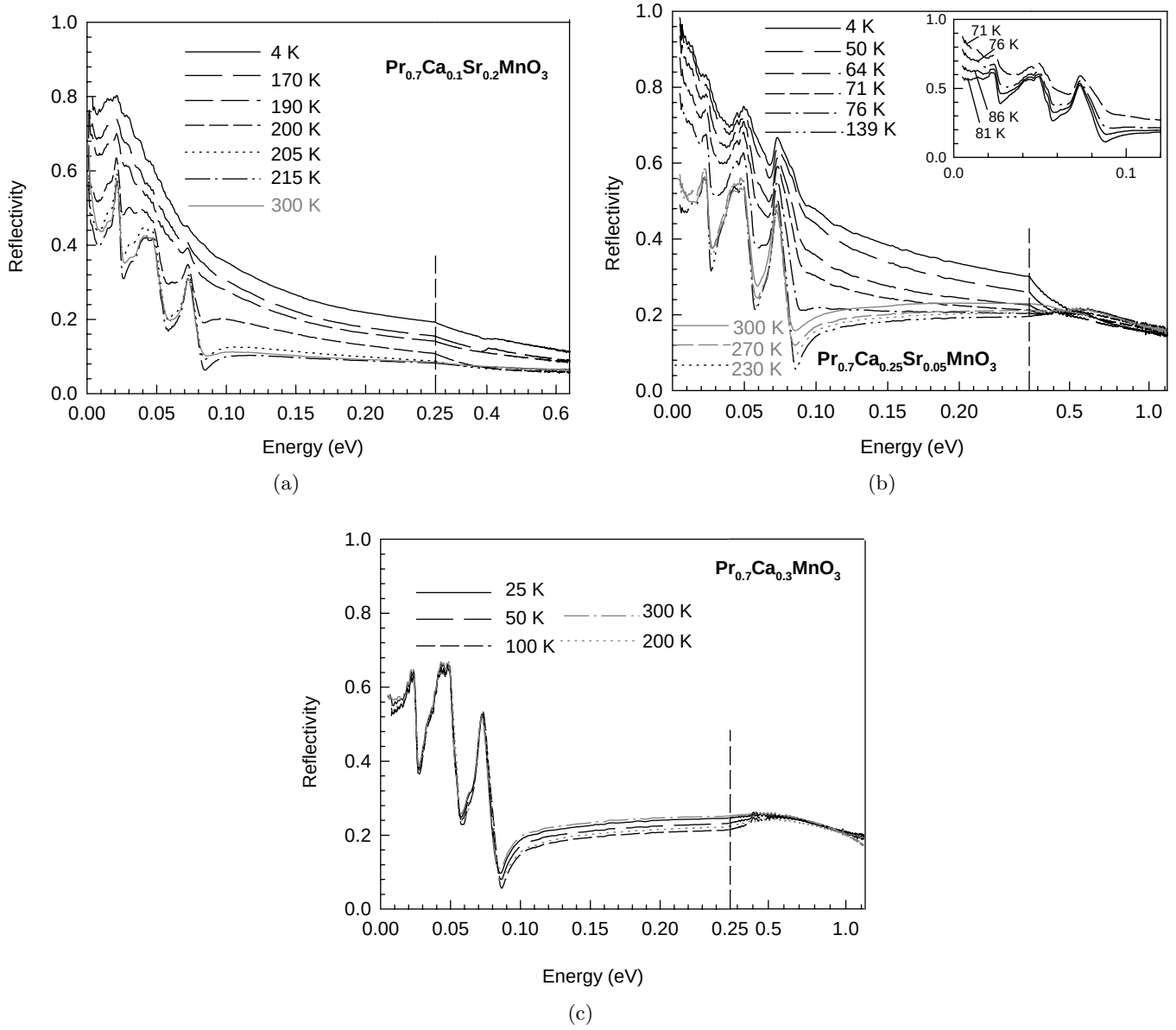

Fig. 2. Temperature dependence of the reflectivity spectrum of sintered ceramics of $Pr_{0.7}Ca_{0.1}Sr_{0.2}MnO_3$ (a) ($T_C \approx 200$ K), $Pr_{0.7}Ca_{0.25}Sr_{0.05}MnO_3$ (b) ($T_C \approx 100$ K), $Pr_{0.7}Ca_{0.3}MnO_3$ (c). Note change of scale at 0.25 eV.

shown in Figure 2c. No transition is observed for this composition.

4 Data fitting and discussion

Once reflectivity spectra are obtained, a procedure currently used is to perform a Kramers-Kronig transformation to obtain the optical conductivity (see *e.g.* the review Ref. [35]). However, this procedure requires the knowledge of the spectrum from zero to infinity, or at least up to regions where there is no more dispersion. To fulfill the mathematical constraints, the application of Kramers-Kronig inversion requires in practice that reflectivity should no longer evolve with frequency on either side of the considered spectral range, or at least can be extrapolated safely down to zero frequency and up to infinity. This requirement is easily fulfilled in insulating samples. Reflectivity spectra can be extrapolated towards asymptotic limits $R_0 = [(\sqrt{\varepsilon_0}-1)/(\sqrt{\varepsilon_0}+1)]^2$, and $R_\infty = [(\sqrt{\varepsilon_\infty}-1)/(\sqrt{\varepsilon_\infty}+1)]^2$. But in conducting media, the dispersion occurs down to zero frequency, and the extrapolation may considerably change both intensity and profile of the low frequency response. We attempted to fit the reflectivity spectra for $x = 0.05$ with a conventional Drude model, with no successful outcome. We then fitted with

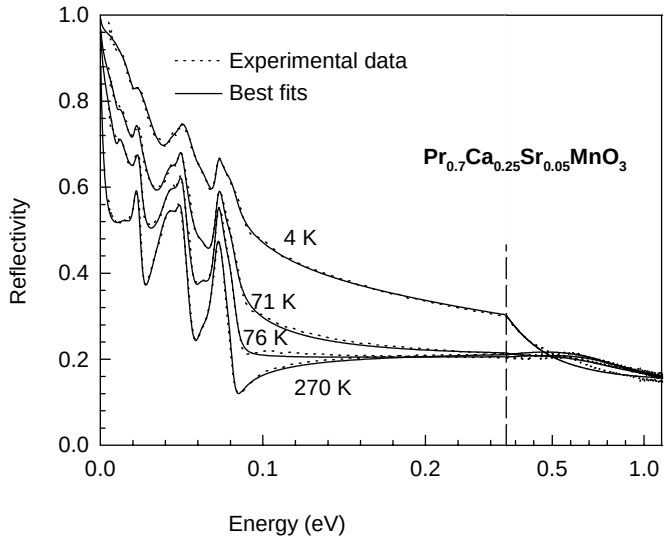

Fig. 3. Examples of best fit (full curves) of the double damping Drude model equation (8) to reflectivity data for $Pr_{0.7}Ca_{0.25}Sr_{0.05}MnO_3$.

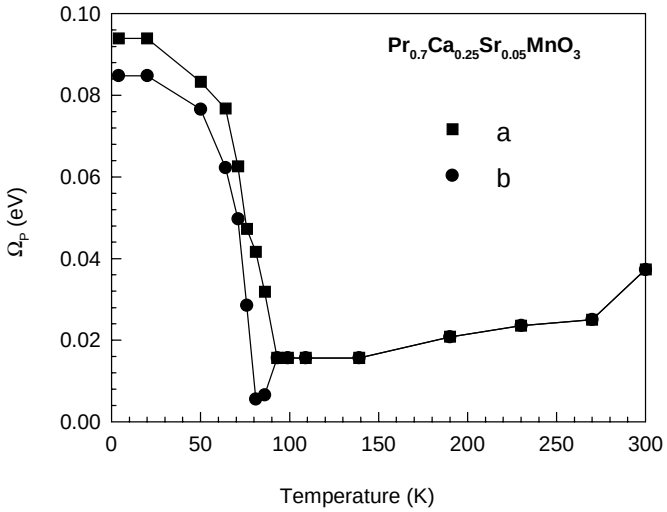

Fig. 5. Temperature dependence of the plasma frequency obtained from both sets of parameters that fit the reflectivity data of $Pr_{0.7}Ca_{0.25}Sr_{0.05}MnO_3$ equally well (see text).

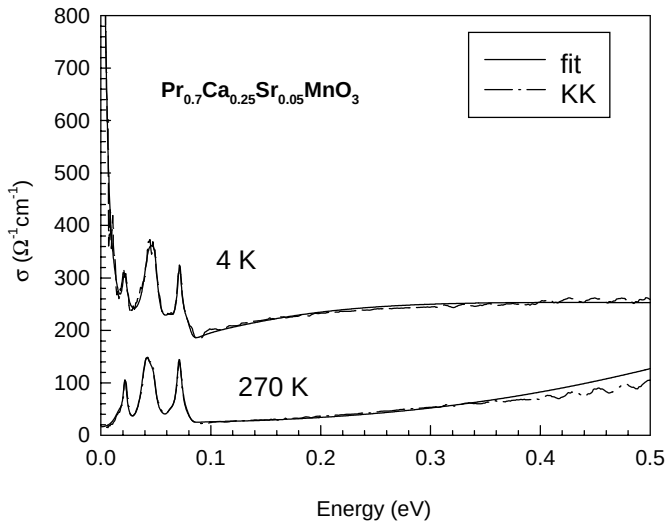

Fig. 4. Comparison of the real part of the optical conductivity obtained by Kramers-Kronig transformation (KK) and from the fit with the double damping Drude model for $Pr_{0.7}Ca_{0.25}Sr_{0.05}MnO_3$.

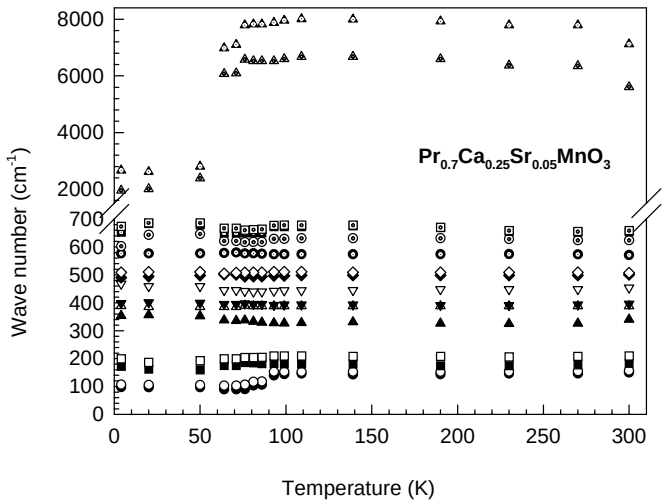

Fig. 6. Temperature dependence of the TO (filled symbols) and LO (open symbols) frequencies in $Pr_{0.7}Ca_{0.25}Sr_{0.05}MnO_3$.

the model equation (8). Typical agreement is shown in Figure 3. We then extrapolated the reflectivity data with additional data points calculated from our best fit extrapolated to zero and performed a KK transformation. The calculated conductivities deduced from KK inversion and best fit compare very well as shown in Figure 4. Actually, two sets of parameters fit the data equally well. One set, labelled (a), emphasizes the low-frequency Drude-like spectral weight, the other, labelled (b), attributes large oscillator strengths to the low-frequency phonons at low temperature, as if they were softened. But, since, within experimental error, the set (a) does not assume mode softening, no conclusion can be drawn. Nevertheless, the temperature dependence of the plasma frequency parameter obtained from either fitting route (a) or (b) is found roughly the same as shown in Figure 5. The plasma frequency sharply increases near the transition temperature and reaches about 0.09 eV at 4 K. The temperature dependence of the TO-LO frequencies (set (a)) is shown in Figure 6. No significant change of phonon frequencies with temperature within experimental uncertainty, is observed, apart from the lower oscillators. Although we have retained the parameter set (a) which does not assume large mode softening (with no significant temperature dependence of oscillator strengths, see Fig. 7), the low-frequency modes seem to shift downwards. On the other hand, there is a net change of behavior of the oscillator that fits the bump in the mid-infrared ($\Omega_{\rm TO} \approx 0.82$ eV). It shifts

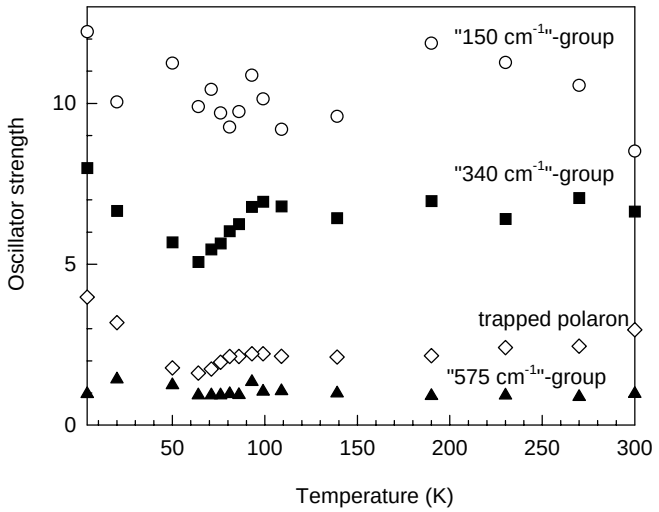

Fig. 7. Evolution of the oscillator strengths *vs.* temperature. The oscillator strengths are summed by groups of peaks at "150 cm^{-1}", "340 cm^{-1}" and 575 cm^{-1}" inherited from the three F_{1u} infrared-active modes of the simple cubic perovskite structure. The fourth plot concerns the trapped polaron signature that lies near 0.8 eV above T_C and drops near 0.24 eV below T_C.

dramatically downwards ($\Omega_{TO} \approx 0.24$ eV) below the transition temperature. The real part of optical conductivity deduced from the best fit of the reflectivity spectra is shown in Figure 8a. We have compared the optical conductivity extrapolated to zero energy to the DC conductivity measured by four-point method. At room temperature, these values quite agree ($\sigma_{293\,K}(\omega \to 0) \approx 15\ \Omega^{-1}\ cm^{-1}$ and $\sigma_{DC\,293\,K} \approx 14\ \Omega^{-1}\ cm^{-1}$). But at 4 K, a large discrepancy is observed ($\omega_{4\,K}(\omega \to 0) \approx 5\ \Omega^{-1}\ cm^{-1}$ while $\sigma_{DC\,4\,K} \approx 1397\ \Omega^{-1}\ cm^{-1}$). Similar discrepancies have been already reported in the literature and ascribed to grain boundary resistivity [6,36].

The fit with double-damping-Drude model equation (8) has the advantage to allow the discrimination of the contribution of charge carrier motion (*i.e.* without restoring force) and the other excitations (oscillators with restoring force like phonons or trapped polarons). It is then straightforward to separate

- the weight of the optical conductivity that is due to the mid-infrared bump;
- what is due to optical phonons shown in Figure 8b;
- and the contribution of mobile charge carriers shown in Figure 8c.

Note that a simple subtraction of spectral weight obtained from KK transformation (an example may be found in Ref. [24]) might be incorrect if excitations are coupled and may give rise, therefore, to Fano-type interference profiles. On the other hand, possible couplings are intrinsically accounted for by the model equation (8). This important point was discussed about nickelates and cuprates in a previous paper [37]. In Figure 8b, the conductivity level related to trapped carriers appears gradually decreased with the decrease of temperature. In Figure 8c, the profile differs greatly from Drude. As for a Drude profile, there is a peak centered at zero energy, but the high-energy conductivity tends to remain a constant throughout the measurement range, not to decrease with increasing frequency as expected from Drude. This is due to the contribution of the non-Drude term $i(\gamma_p - \gamma_0)\omega$ in equation (8), while the best fit implies $\gamma_0 \ll \gamma_p$. This means that the response does show strong departure from conventional Drude. The conductivity of mobile charge carriers appears nearly flat in the 0.1–1 eV energy range, what may be attributed to incoherent scattering instead of coherent motion in the Drude sense. The oscillator strength of the mid-infrared bump is plotted in Figure 7. The oscillator strength decreases upon decreasing temperature near T_C (see also Fig. 8b). Below T_C, one cannot decide whether the bump is abruptly shifted downward with an oscillator strength that increases upon cooling, or if the bump of the upper phase is progressively replaced by a lower-energy peak. In any case, this behavior that is revealed by our fitting approach has not been reported before to our knowledge, probably because the signature was merged in the Drude-like response obtained by KK analysis. The plot of Ω_p^2, a quantity that normally scales with the spectral weight of mobile charge carriers, *versus* temperature, is shown in Figure 9. The scaling of Ω_p^2 with the spectral weight of mobile charge carriers is confirmed in Figure 9, unambiguously. In addition, one observes upon cooling first a decrease of Ω_p^2, then a huge increase below T_C, qualitatively (but not quantitatively, presumably due to inter-grain effects) consistent with the behavior of the DC resistivity shown in Figure 1. This behavior is somewhat different from that of the sole parameter that was considered in the literature, N_{eff}, the effective number of charge carriers obtained by integrating the spectral conductivity from zero to an energy cutoff $\hbar\omega_c$

$$\int_0^{\omega_c} \sigma(\omega')\mathrm{d}\omega' = \frac{\pi e^2}{2}\frac{N_{eff}(\omega)}{m^*} \qquad (9)$$

where e is the electron charge and m^* the electron effective mass. The temperature dependence of the ratio N_{eff}/N, where N is the number of manganese ions per unit volume (N is taken as roughly the same as for a cubic system with $a \sim 3.82$ Å, $N \sim 1.8 \times 10^{22}$ e/cm^3), is plotted in Figure 10. The electron mass has been assumed for m^*. The phonon contribution is obviously excluded from the integration. The profile of the integrated conductivity appears significantly different from that of Ω_p^2, what is not surprising since the latter concerns mobile charge carriers only, whereas the former includes both mobile and trapped charge carriers. For $\Omega_c = 0.1$ eV, the profile of the integrated conductivity is quite similar with $\Omega_p^2(\omega)$, which is proportional to the Drude weight ($\varepsilon_\infty \Omega_p^2(\omega)$ with $\varepsilon_\infty = cte \approx 4.9$). Indeed, the mid-IR band scarcely contributes to the conductivity below 0.1 eV and the integrated conductivity is then principaly due to the plasmon described by equation (4). This study confirms

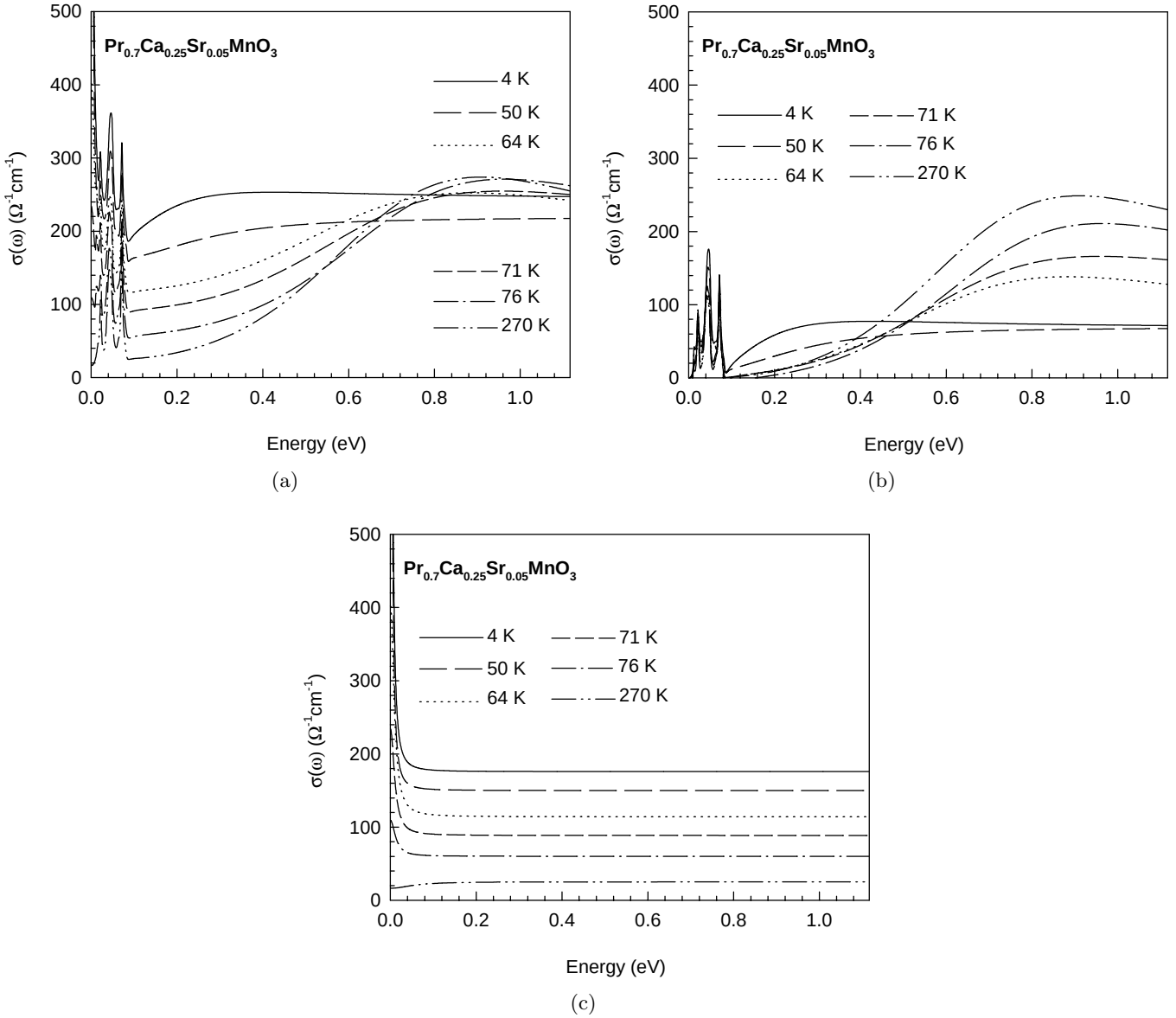

Fig. 8. Real part of the spectral conductivity deduced from the double damping Drude fit of the $Pr_{0.7}Ca_{0.25}Sr_{0.05}MnO_3$ reflectivity data (a). The oscillatory components (b) are straightforwardly discriminated from the plasmon contribution (c).

the general trends already reported in the literature that may be summarized as follows:

- In the upper non-ferromagnetic phase, the spectral conductivity mainly consists of a 0.8 eV band (see Fig. 11), assigned to a polaron related to the Jahn-Teller effect of Mn^{3+}. We emphasize an additional contribution to the conductivity described in terms of extended "double-damping" Drude model, with a plasma frequency that increases with temperature, consistent with the tendency at localization which dominates the transport properties in this phase;
- upon decreasing temperature in the upper phase, the spectral weight of this 0.8 eV absorption tends to decrease. This phenomenon is revealed by our fitting procedure, whereas it was masked in the reports *via* sole KK inversion;
- the change of regime of electronic transport upon cooling below T_C which manifests itself by a progressive shift from trapped-polaron-dominated conductivity in the upper phase to mobile-polaron-dominated (incoherent scattering) conductivity at low temperature, the non-dominant contribution being non-zero at all temperatures. The measurement of each contribution (mobile and trapped species) allows a more precise parameterization and analysis, compared to those solely based upon KK transformation.

To summarize, we have measured and carefully analyzed the temperature dependence of the infrared

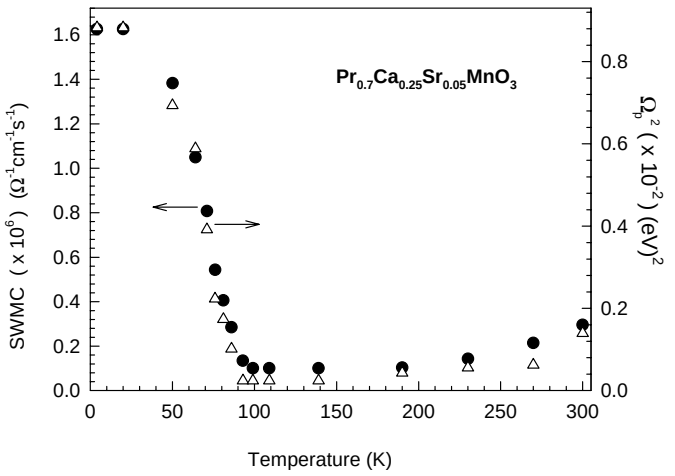

Fig. 9. Comparison between the temperature dependence of the spectral weight of the mobile carriers (SWMC) obtained by integration of the conductivity curves shown in Figure 8c till the cut-off frequency $\omega_c = 1.1$ eV, and of the squared plasma frequency (quantity proportional to the free carrier density), in $Pr_{0.7}Ca_{0.25}Sr_{0.05}MnO_3$. The contribution of the trapped polaron, already shown in Figure 7, is not shown here.

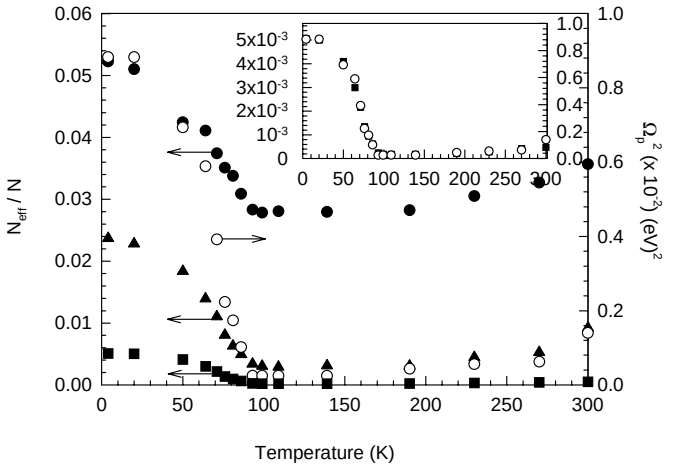

Fig. 10. Temperature dependence of $N_{\rm eff}/N$ deduced from integration of the part of the conductivity due to the plasmon and the trapped polaron band (phonons are excluded) till cut-off frequency $\omega_c = 0.1$ eV (filled squares), 0.5 eV (filled circles) and 1.1 eV (triangles) in $Pr_{0.7}Ca_{0.25}Sr_{0.05}MnO_3$. Comparison with the temperature dependence of the plasma frequency squared (open circles). In the insert, $N_{\rm eff}(\omega_c = 0.1\ {\rm eV})/N$ normalized with Ω_p^2.

reflectivity of $Pr_{0.7}Ca_{0.25}Sr_{0.05}MnO_3$, a composition that displays both large conductivity jump and CMR phenomenon [3–5]. The analysis we have detailed allows, among other advantages, an unambiguous discrimination between mobile and trapped charge carriers. We have thus been able to quantify the actual temperature dependence of each contribution, which was not clear in the literature [16–27], and may help at better comparison with theoretical models in this field [11,38,39].

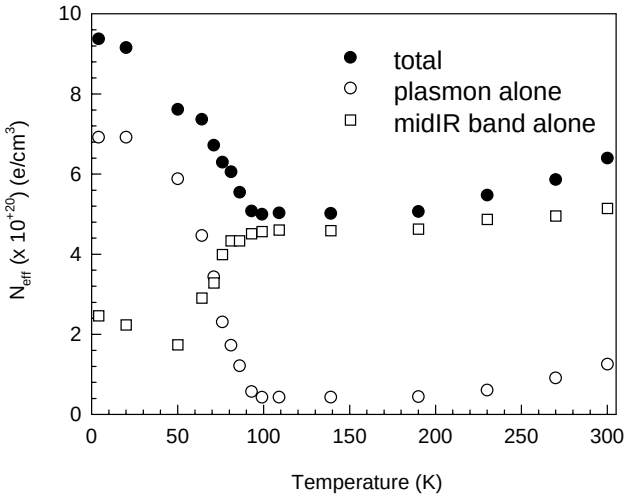

Fig. 11. $N_{\rm eff}$ ($\omega_c = 1.1$ eV) calculated from equation (9) considering the total conductivity (filled circles), the plasmon alone expressed by equation (4) (empty circles) and the mid-IR band equation (7) (empty squares). The phonon contribution is excluded from the integration.

The help of A. Blin and D. de Sousa, CRMHT, CNRS, Orléans, is gratefully acknowledged.

References

1. R. von Helmot, J. Wecker, B. Holzapfel, L. Schultz, K. Samwer, Phys. Rev. Lett. **71**, 2331 (1993).
2. S. Jin, T.H. Tiefel, M. McCormack, R. Fastnacht, R. Ramesh, L.H. Chen, Science **264**, 13 (1994).
3. J. Hetmanek, Z. Jirak, D. Sedmidubsky, A. Maignan, Ch. Simon, V. Caignaert, C. Martin, B. Raveau, Phys. Rev. B **54**, 11947 (1996).
4. B. Raveau, A. Maignan, Ch. Simon, J. Solid State Chem. **117**, 424 (1995).
5. A. Maignan, Ch. Simon, V. Caignaert, B. Raveau, Z. Phys. B **99**, 305 (1996).
6. C.N.R. Rao, B. Raveau, in *Colossal Magnetoresistance, Charge Ordering and Related Properties of Manganese Oxides* (World Scientific, 1998).
7. G.M. Zhao, M.B. Hunt, H. Keller, Phys. Rev. Lett. **78**, 955 (1997); G.M. Zhao, M.B. Hunt, K. Conder, H. Keller, K.A. Müller, Physica C **282**, 202 (1997).
8. J.S. Zhou, W. Archibald, J.B. Goodenough, Nature **381**, 770 (1996).
9. V.Z. Krezin, S.A. Wolf, Philos. Mag. B **76**, 241 (1997).
10. J.M. De Teresa *et al.*, Nature **386**, 256 (1997).
11. A.J. Millis, R. Mueller, B.I. Shraiman, Phys. Rev. B **54**, 5405 (1996).
12. D. Eagles, R.P.S.M. Lobo, F. Gervais, Phys. Rev. B **52**, 6440 (1995).
13. T. Katsufuji, T. Tanabe, T. Ishikawa, Y. Fukuda, T. Arima, Y. Tokura, Phys. Rev. B **54**, 14230 (1996).
14. R.P.S.M. Lobo, F. Gervais, S.B. Oseroff, Europhys. Lett. **37**, 341 (1997).
15. P. Calvani, A. Paolone, P. Dore, S. Lupi, P. Maselli, P.G. Medaglia, Phys. Rev. B **54**, R9592 (1996).

16. K.H. Kim, J.Y. Gu, H.S. Choi, G.W. Park, T.W. Noh, Phys. Rev. Lett. **77**, 1877 (1996).
17. K.H. Kim, J.Y. Gu, H.S. Choi, D.J. Eom, J.H. Jung, T.W. Noh, Phys. Rev. B **55**, 4023 (1997).
18. K.H. Kim, J.H. Jung, T.W. Noh, J. Korean Phys. Soc. **32**, S1832 (1998).
19. K.H. Kim, J.H. Jung, T.W. Noh, Phys. Rev. Lett. **81**, 1517 (1998).
20. K.H. Kim, J.H. Jung, D.J. Eom, T.W. Noh, Jaejun Yu, E.J. Choi, Phys. Rev. Lett. **81**, 4983 (1998).
21. H.L. Liu, S.L. Cooper, S.-W. Cheong, Phys. Rev. Lett. **81**, 4684 (1998).
22. M. Quijada, J. Cerne, H.D. Drew, K.H. Ahn, A.J. Millis, R. Shreekala, R. Ramesh, M. Rajeswari, T. Venkatesan, Phys. Rev. **58**, 16093 (1998).
23. S. Yoon, H.L. Liu, G. Schollerer, S.L. Cooper, P.D. Han, D.A. Payne, S.-W. Cheong, Z. Fisk, Phys. Rev. B **58**, 2795 (1998).
24. Y. Okimoto, T. Katsufuji, T. Ishikawa, T. Arima, T. Tokura, Phys. Rev. B **55**, 4206 (1997).
25. Y. Okimoto, Y. Tomioka, Y. Onose, Y. Otsuka, Y. Tokura, Phys. Rev. B **57**, R9377 (1998).
26. A.V. Boris, N.N. Kovaleva, A.V. Bazhenov, P.J.M. van Bentum, Th. Rasing, S.-W. Cheong, A.V. Samoilov, N.-C. Yeh, Phys. Rev. B **59**, R697 (1999).
27. A.V. Boris, N.N. Kovaleva, A.V. Bazhenov, A.V. Samoilov, N.-C. Yeh, R.P. Vasquez, J. Appl. Phys. **81**, 5756 (1997).
28. J.F. Baumard, F. Gervais, Phys. Rev. B **15**, 2316 (1977).
29. F. Gervais, in *Infrared and Millimeter Waves*, edited by K.J. Button (Academic Press, New York, 1983), Vol. 8, pp. 279-339.
30. F. Gervais, P. Echegut, J.M. Bassat, P. Odier, Phys. Rev. B **37**, 9364 (1988).
31. R.P.S.M. Lobo, F. Gervais, C. Champeaux, P. Marchet, A. Catherinot, Mat. Sci. Engineer. B **34**, 74 (1995).
32. F. Gervais, B. Piriou, J. Phys. C **7**, 2374-86 (1974).
33. T. Kurosawa, J. Phys. Soc. Jpn **16**, 1298 (1961).
34. F. Gervais, C. Daulan, A. Maignan, R.P.S.M. Lobo, Int. J. Mod. Phys. **12**, 3393 (1998).
35. D.B. Tanner, T. Timusk, in *Physical Properties of High Temperature Superconductors*, edited by D.M. Ginsberg (World Scientific, 1992), Vol. III, pp. 363-469.
36. H.Y. Hwang, S.-W. Cheong, N.P. Ong, B. Batlogg, Phys. Rev. Lett. **77**, 2041 (1996).
37. F. Gervais, R.P.S.M. Lobo, M. Licheron, F.J. Gotor, Ferroelectrics **177**, 107 (1996).
38. C. Zener, Phys. Rev. **82**, 403 (1951); P.W. Anderson, H. Hasegawa, Phys. Rev. **100**, 675 (1955); P.G. de Gennes, Phys. Rev. **118**, 141 (1960).
39. H. Röder, J. Zhang, A.R. Bishop, Phys. Rev. Lett. **76**, 1356 (1996).